

Mechanisms and Machine Science

Enrico Ciulli

Alessandro Ruggiero *Editors*

# Proceedings of ITS-IFTToMM 2024


5<sup>th</sup> International Tribology Symposium  
of IFTToMM



 Springer

The Springer logo, which consists of a white chess knight icon on a pedestal, followed by the word "Springer" in a white serif font.

## Series Editor

Marco Ceccarelli , *Department of Industrial Engineering, University of Rome Tor Vergata, Roma, Italy*


## Advisory Editors

Burkhard Corves, *RWTH Aachen University, Aachen, Germany*

Victor Glazunov, *Mechanical Engineering Research Institute, Moscow, Russia*

Alfonso Hernández, *University of the Basque Country, Bilbao, Spain*

Tian Huang, *Tianjin University, Tianjin, China*

Juan Carlos Jauregui Correa , *Universidad Autonoma de Queretaro, Queretaro, Mexico*

Yukio Takeda, *Tokyo Institute of Technology, Tokyo, Japan*

Sunil K. Agrawal, *Department of Mechanical Engineering, Columbia University, New York, NY, USA*

This book series establishes a well-defined forum for monographs, edited Books, and proceedings on mechanical engineering with particular emphasis on MMS (Mechanism and Machine Science). The final goal is the publication of research that shows the development of mechanical engineering and particularly MMS in all technical aspects, even in very recent assessments. Published works share an approach by which technical details and formulation are discussed, and discuss modern formalisms with the aim to circulate research and technical achievements for use in professional, research, academic, and teaching activities.

This technical approach is an essential characteristic of the series. By discussing technical details and formulations in terms of modern formalisms, the possibility is created not only to show technical developments but also to explain achievements for technical teaching and research activity today and for the future.

The book series is intended to collect technical views on developments of the broad field of MMS in a unique frame that can be seen in its totality as an Encyclopaedia of MMS but with the additional purpose of archiving and teaching MMS achievements. Therefore, the book series will be of use not only for researchers and teachers in Mechanical Engineering but also for professionals and students for their formation and future work.

The series is promoted under the auspices of International Federation for the Promotion of Mechanism and Machine Science (IFToMM).

Prospective authors and editors can contact Mr. Pierpaolo Riva (publishing editor, Springer) at: [pierpaolo.riva@springer.com](mailto:pierpaolo.riva@springer.com)

Indexed by SCOPUS and Google Scholar.

Enrico Ciulli · Alessandro Ruggiero  
Editors

# Proceedings of ITS-IFTToMM 2024

5<sup>th</sup> International Tribology Symposium  
of IFTToMM

*Editors*

Enrico Ciulli  
Department of Civil and Industrial  
Engineering  
University of Pisa  
Pisa, Italy

Alessandro Ruggiero  
Department of Industrial Engineering  
University of Salerno  
Fisciano, Italy

ISSN 2211-0984

ISSN 2211-0992 (electronic)

Mechanisms and Machine Science

ISBN 978-3-031-62615-9

ISBN 978-3-031-62616-6 (eBook)

<https://doi.org/10.1007/978-3-031-62616-6>

© The Editor(s) (if applicable) and The Author(s), under exclusive license  
to Springer Nature Switzerland AG 2024

This work is subject to copyright. All rights are solely and exclusively licensed by the Publisher, whether the whole or part of the material is concerned, specifically the rights of translation, reprinting, reuse of illustrations, recitation, broadcasting, reproduction on microfilms or in any other physical way, and transmission or information storage and retrieval, electronic adaptation, computer software, or by similar or dissimilar methodology now known or hereafter developed.

The use of general descriptive names, registered names, trademarks, service marks, etc. in this publication does not imply, even in the absence of a specific statement, that such names are exempt from the relevant protective laws and regulations and therefore free for general use.

The publisher, the authors and the editors are safe to assume that the advice and information in this book are believed to be true and accurate at the date of publication. Neither the publisher nor the authors or the editors give a warranty, expressed or implied, with respect to the material contained herein or for any errors or omissions that may have been made. The publisher remains neutral with regard to jurisdictional claims in published maps and institutional affiliations.

This Springer imprint is published by the registered company Springer Nature Switzerland AG  
The registered company address is: Gewerbestrasse 11, 6330 Cham, Switzerland

If disposing of this product, please recycle the paper.

# Preface

This book contains the Proceedings of the 5<sup>th</sup> International Tribology Symposium of IFToMM, the International Federation for the Promotion of Mechanism and Machine Science, ITS-IFTToMM 2024, held from May 6<sup>th</sup> to 8<sup>th</sup>, 2024, in Salerno, Italy, jointly with the 9<sup>th</sup> AIT (Italian Tribology Association) Workshop “Tribology and Industry” (May 8<sup>th</sup>–9<sup>th</sup>, 2024).

The 5<sup>th</sup> ITS-IFTToMM follows the 1<sup>st</sup> edition held in Beijing, China, in 2008, the 2<sup>nd</sup> one held in Rio de Janeiro, Brazil, in 2010, the 3<sup>rd</sup> one held in Luleå, Sweden, in 2013, and the 4<sup>th</sup> one held in Jeju, Korea, in 2017. It is the first in presence Conference organized by the Technical Committee for Tribology of IFToMM after the COVID years.

The aim of ITS-IFTToMM 2024 has been to provide the opportunity for scientists, engineers, and students from all over the world, both from academia and industry, to come together and exchange the latest information on a wide range of topics relevant to tribology.

This book collects 48 peer-reviewed papers on the major themes of tribology and other related fields such as friction, wear, lubrication, lubricants, biotribology, tribomaterials, solid lubricants, surface engineering, tribotesting, modeling in tribology, contact mechanics, micro/nanotribology, tribology in power generating systems, metal working tribology, tribology in road transport and tribology in medicine. The Proceedings are divided into six chapters, essentially reflecting the technical sessions of the Symposium: friction corrosion and wear, coatings, bearings, optimization of mechanical systems, contact mechanics and viscoelasticity, bio/green tribology.

We would like to express our sincere gratitude to everyone who contributed to the success of the Symposium, particularly all the authors for their interesting scientific contributions, the reviewers for their useful feedback, all the members of the Scientific and Organizing Committees for their valuable work, and all people of Springer for their efficient support in publishing this book.

Enrico Ciulli  
Alessandro Ruggiero

# Contents

## Friction, Corrosion and Wear

Experimental Wear Analysis on Mechanical Seals for Concrete Mixers .....	3
<i>Silvia Logozzo and Maria Cristina Valigi</i>	
Clarification of the Corrosion and Frictional Behavior of Nitrogen-Doped ta-C Coating in Nitride Acid Solution .....	13
<i>Ruixi Zhang, Haodong Feng, Noritsugu Umehara, and Takayuki Tokoroyama</i>	
Laboratory Linear Friction Tester: Design and Results .....	23
<i>Emanuele Lenzi, Flavio Farroni, Aleksandr Sakhnevych, Francesco Timpone, and Andrea Genovese</i>	
Experimental Investigation on Tire-Road Interaction Made with the British Pendulum Evo as Thermal Conditions of the Tire and Road Surface .....	31
<i>Fabio Romagnuolo, Stefano Avolio, Raffaele Maglione, Raffaele Stefanelli, and Guido Napolitano dell'Annunziata</i>	
Influence of the Counter-Body Material on Micro-Abrasion-Corrosion .....	41
<i>José Daniel Biasoli de Mello, Miguel Angel Narvaes Ardila, and Henara Lilian Costa</i>	
Tribocorrosive Analysis of Titanium Grade V in Different Biological Solutions .....	54
<i>Marco De Stefano, Alessandro Sicilia, and Alessandro Ruggiero</i>	
Pin-on-Disk Wear Investigation on Bronze Coating – Part 1: Definition of the Test Methodology .....	65
<i>Enrico Ciulli and Eugeniu Grabovic</i>	
Pin-on-Disk Wear Investigation on Bronze Coating – Part 2: Analysis of the Experimental Results .....	77
<i>Eugeniu Grabovic and Enrico Ciulli</i>	
Evaluation the Tribological Properties of Different Fiber Reinforced Polymers .....	85
<i>Mircea Cioaza, Corina Birleanu, Marius Pustan, Paul Bere, and Glad Contiu</i>	

**Coatings**

- Development of Low-Friction Technology for Treating Nitrogen-Containing Diamond-Like Carbon Coatings in Ambient Air Using Dielectric Barrier Discharge ..... 99  
*Wenjun Wu, Noritsugu Umehara, Takayuki Tokoroyama, Motoyuki Murashima, and Ruixi Zhang*
- Advancing Tribological Understanding: Insights into In-Plane Wear and Edge Friction Mechanisms of Graphene and Its Derivatives ..... 107  
*Yilong Jiang, Lei Chen, Chuan Tang, Yangqin Liu, Wenmeng Yan, Liang Wei, and Linmao Qian*
- Friction and Wear Properties of Super-Hydrophobic Diamond-Like Carbon (DLC) Coating ..... 116  
*Young-Jun Jang, Hiroyuki Kousaka, and Noritsugu Umehara*
- Friction Coefficient of the PVD-AlCrN Coated Cemented Carbide and Hardened Steel Tribo-Pair Under Dry Sliding ..... 124  
*Krishna Chaitanya Solasa, N. V. Venkataraman, Palash Roy Choudhury, and Abhijit Bhattacharyya*
- Tribological Behavior of ta-C Coating Originated by Surface Defects ..... 134  
*WooYoung Lee, Jae-Il Kim, Young-Jun Jang, and Noritsugu Umehara*
- Surface Fatigue of DLC-Coated Spur Gears ..... 140  
*Remigiusz Michalczewski, Marek Kalbarczyk, Maciej Łuszcz, Daniel Pieniak, Emilia Skotek, Jakub Nędza, and Andrzej N. Wieczorek*
- Effect of Hydrogen Doping for ta-C on Friction of ta-C:H Sliding Against Bearing Steel in High Temperature and High Vacuum ..... 149  
*Ruixi Zhang, Daiki Yasuda, Noritsugu Umehara, and Takayuki Tokoroyama*
- Enhancing Cutting Tool Performance through ta-C:Ta Coating for CFRP Dry Machining: Investigation of Wear Resistance and Cutting Forces ..... 159  
*Kosuke Suzuki, Takayuki Tokoroyama, Riko Takita, Ruixi Zhang, Noritsugu Umehara, Shun Sato, and Shin Nishida*

**Bearings**

- Optimization of a Herringbone Grooved Thrust Bearing ..... 171  
*Federico Colombo, Edoardo Goti, Luigi Lentini, and Andrea Trivella*



Investigation on the Static Characteristics of a Dynamic Gas Thrust Bearing with Spiral Grooves for a Small-Scale High-Speed Application . . . . .	180
<i>Federico Colombo, Edoardo Goti, Luigi Lentini, and Terenziano Raparelli</i>	
Effect of Bearing Edges Chamfering on the Characteristics of a Wide Range of Journal Bearing Ratio Under 3D Misalignment . . . . .	191
<i>Hazim U. Jamali, Adolfo Senatore, Muhsin Jaber Jweeg, H. S. S. Aljibori, M. N. Mohammed, Oday I. Abdullah, and M. Alfiras</i>	
Analysis of the Dynamic Response of Variable Bearing Design Under Impact Load Using Taguchi Method . . . . .	202
<i>Hazim U. Jamali, Moneer H. Tolephih, Muhsin Jaber Jweeg, H. S. S. Aljibori, M. N. Mohammed, Oday I. Abdullah, M. Alfiras, and Alessandro Ruggiero</i>	
Temperature Profile at Pad's Leading Edge of a Tilting-Pad Journal Bearing: CFD Modeling and Experimental Validation . . . . .	213
<i>Steven Chatterton, Andrea Riva, Edoardo Gheller, Ludovico Dassi, Andrea Vania, and Paolo Pennacchi</i>	
Comparison Between Numerical and Experimental Static Performance and Sensitivity Study on a Tilting Pad Journal Bearing in a Load on Pad Configuration . . . . .	223
<i>Alberto Betti, Paola Forte, Luis San Andrés, Adolfo Delgado, and Enrico Ciulli</i>	
Acoustic Emission-Based Detection of Starved Conditions to Prevent Adhesive Wear Damage in Journal Bearings . . . . .	235
<i>Florian König, Florian Wirsing, and Benjamin Klinghart</i>	
<b>Design and Optimization of Mechanical Systems</b>	
Contact Force Recognition in Robotic Fingertips' Interface . . . . .	247
<i>Gabriele Maria Achilli, Virginia Burini, Silvia Logozzo, and Maria Cristina Valigi</i>	
Advantages and Limitations of Oil Film Thickness Capacitive Sensor Measurements in Balanced Vane Pumps . . . . .	257
<i>Caterina Natali, Umberto Stuppioni, Mattia Battarra, Alessandro Blum, Giorgio Dalpiaz, and Emiliano Mucchi</i>	
Dynamic and Stability Analysis of an Air Pad Controlled by a Differential Diaphragm Valve . . . . .	267
<i>Federico Colombo, Luigi Lentini, Terenziano Raparelli, and Andrea Trivella</i>	

On the Dynamic Characterization of Elastomeric O-Rings .....	277
<i>Federico Colombo, Roberto Ghidini, and Luigi Lentini</i>	
Preliminary Development of a Fluidic Device for Astrobiology Missions .....	287
<i>Gabriele Maria Achilli, Sebastiano Angelella, Marco Dionigi, Silvia Logozzo, and Maria Cristina Valigi</i>	
Necessity of the Tire Temperature-Dependant Parameters in Vehicle Virtual Sensing .....	296
<i>Mario Barbaro, Fabio Romagnuolo, Flavio Farroni, Francesco Timpone, and Aleksandr Sakhnevych</i>	
Thermo-Mechanical Investigation of a Rotational Friction Joint Under High-Frequency Excitation .....	306
<i>Simon Keller and Alexander Fidlin</i>	
Dynamic Simulation of the Multibody Model of the Rabinowicz Test for Friction Modeling in the SIMSCAPE Environment .....	316
<i>Carmine Maria Pappalardo, Ömer Ekim Genel, Rosario La Regina, and Domenico Guida</i>	
Analysis of the Friction Impact on the Performance of the Linear Quadratic Regulator Controller Applied to the Multibody Model of the Furuta Pendulum .....	325
<i>Carmine Maria Pappalardo, Rosario La Regina, Ömer Ekim Genel, and Domenico Guida</i>	
Analysis and Modeling of a Mechanical Power Recirculating Test Bench for Gears Testing .....	336
<i>Marco Claudio De Simone, Salvio Veneziano, and Domenico Guida</i>	
<b>Contact Mechanics and Viscoelasticity</b>	
Non-Invasive Experimental Investigation for Time-Temperature Superposition Shift Factor Estimation in Viscoelastic Materials Characterization .....	347
<i>Raffaele Maglione, Stefano Avolio, Guido Napolitano Dell'Annunziata, Marco Ruffini, and Andrea Genovese</i>	
Topography Measurements Analysis Between Road Surfaces and Their Silicone Replicas .....	357
<i>Stefano Avolio, Emanuele Lenzi, Guido Napolitano Dell'Annunziata, Marco Ruffini, and Andrea Genovese</i>	

An Enhanced Greenwood-Williamson Contact Model for the Evaluation of Local Tire/Road Contact Area .....	367
<i>Raffaele Stefanelli, Mario Barbaro, Aleksandr Sakhnevych, Francesco Timpone, and Flavio Farroni</i>	
A Superellipse-Based Model for Tire Contact Patches Reproduction .....	377
<i>Marco Ruffini, Mario Barbaro, Fabio Romagnuolo, Raffaele Stefanelli, and Guido Napolitano Dell'Annunziata</i>	
The Interplay of Viscoelasticity and Friction in Thin Tape Peeling .....	387
<i>Marco Ceglie, Nicola Menga, and Giuseppe Carbone</i>	
Viscoelastic Circular Contact Mechanics: A Boundary Element Formulation .....	395
<i>Michele Santeramo, Carmine Putignano, Stefan Krenn, Georg Vorlauffer, and Giuseppe Carbone</i>	
Modelling Viscoelastic Adhesion and Friction in Sliding Contact Mechanics .....	406
<i>Cosimo Mandriota, Giuseppe Carbone, and Nicola Menga</i>	
Modelling Cavitation in Viscoelastic Thin Lubricating Films .....	416
<i>Humayun Ahmed and Luca Biancofiore</i>	
<b>Bio/Green Tribology</b>	
Antifrictional Effect of Biobased Fillers on Bioceramic Alumina .....	429
<i>Tadas Matijošius, Audrius Žunda, Laurynas Staišiūnas, Aušra Selskienė, and Juozas Padgurskas</i>	
Experimental Analysis of Different Dental Implants Surfaces by Using Optical Methods .....	439
<i>Marco De Stefano, Antonio Lanza, Alessandro Sicilia, and Alessandro Ruggiero</i>	
Tribological Behaviour of PLA Composites with Different Natural Fibers and Degradation Mechanisms .....	450
<i>Marco De Stefano, Alessandro Sicilia, Petr Valášek, Roberto D'Amato, and Alessandro Ruggiero</i>	
Tribological Investigations of Waste Cooking Palm Oil Using Them for Production of Lubricants .....	460
<i>Juozas Padgurskas, Raimundas Rukuiža, Darius Volskis, Andrius Karalis, and Adolfo Senatore</i>	

**From Marker Trajectories to Muscular Activations: A Musculoskeletal  
Multibody Model Considering Compliant Tendon Behaviour** ..... 468  
*Alessandro Sicilia, Marco De Stefano, and Alessandro Ruggiero*

**On the Tribological Performance of Vegetable Lubricants: Experimental  
Investigation on Rice Bran Oil with Propyl Gallate** ..... 479  
*Roberto D'Amato, Antonio Nieto-Marquez Ballesteros,  
Alessandro Sicilia, Marco De Stefano, and Alessandro Ruggiero*

**Author Index** ..... 489

# **Friction, Corrosion and Wear**



# Experimental Wear Analysis on Mechanical Seals for Concrete Mixers

Silvia Logozzo and Maria Cristina Valigi<sup>(✉)</sup>

Università degli Studi di Perugia, Via G. Duranti, Perugia, Italy  
mariacristina.valigi@unipg.it

**Abstract.** The paper presents an experimental wear analysis of a mechanical face seal for twin-shaft concrete mixers. The studied mechanical seals are lubricated through a timed pump which delivers grease progressively and distributes the required amount of lubricant to each seal evenly. Seals aim at preventing the leakage of the dough from the tank of the concrete mixer through the gaps between the fixed and rotating parts. To prevent the dough from spilling out, the flow is contrasted by adding lubricating grease. The seals, after a certain period of operation, exhibit significant wear progress due to an interlayer of concrete/inert material. The experimental wear analysis is carried out with the aid of 3D scanners and from the observation of the results, three different phases are defined during the material removal, considering different wear behaviors. Results are also compared to wear volumes from gravimetric tests. Therefore, this paper lays the groundwork for a future model of the wear behaviour of mechanical face seals in twin-shaft concrete mixers and for proposing solutions to limit and control the wear phenomena.

**Keywords:** Green Tribology · Mechanical Face Seal · Wear · 3D Scanners · Concrete Mixers

## 1 Introduction

Mechanical seals are employed in various industrial applications such as machinery construction, production of equipment, land or sea transportation, rotating axles, agricultural machinery, mining machinery, etc. They are indispensable components for the proper functioning of the machines in which they are installed as they have the function of preventing fluid leakages [1–6]. The knowledge of the wear behavior of seals' interfaces is particularly important to improve their design enhancing their useful life and meeting the increasingly required sustainable development goals (SDG) [7]. In fact, wear assessment is a topic of significant importance in green tribology and can be extremely helpful to obtain and determine all the information needed to effectively re-design components and detect damages in machinery, components, infrastructure, etc. [8].

In this paper the wear of a mechanical face seal for a twin-shaft concrete mixer is studied. The concrete mixer where the seal is mounted was already described in [9, 10]. These kinds of seals must have a long service life to ensure maximum isolation and reliability as many other components [11, 12].

The purpose of the studied mechanical face seal is to prevent the slurry from leaking out of the tank through the gaps between the fixed and rotating parts. The lubricating action of the grease creates a film of grease at the interface between the two mating surfaces, keeping the two rings in mediated contact. In the studied concrete mixer, a timed pump delivers lubricant progressively and cyclically at the seal's interface, so that there is a phase of full lubrication and a phase of boundary lubrication.

In this work, the wear of the seal that occurs during the boundary lubrication phase is evaluated using a 3D scanner and applying one of the methods described in [13] and in particular the technique used for the mixing blades in [14]. Results are also compared to wear volumes from gravimetric tests.

3D scanners can be advantageously employed for a variety of applications such as inspections [15, 16], evaluations of contact [17], biomechanical applications [18, 19] and wear assessments in all the sectors [20]. In the first part of the paper, the studied seals and concrete mixers are described with attention to how the lubrication is delivered. In the second part, the experimental results obtained for the worn seal with the use of a 3D scanner and related methods are presented and discussed.

The analysis of results allowed the identification of three different wear phases occurring during the lifetime of the studied seal distinguishing three different wear behaviors.

## 2 Mechanical Face Seals in Twin Shaft Concrete Mixers

### 2.1 Description of the Mechanical Face Seals

The studied mechanical face seal is a component of a twin shaft concrete mixer that has four identical mechanical face seals, two for each shaft.

The purpose of these seals is to prevent or limit the leakage of dough from the tank avoiding damage to the shaft bearings and planetary gears. The mechanical face seals have three main components: the metallic ring, the plastic ring made of polyester, and the coupling ring. The coupling ring has the function of guaranteeing the contact between the mating faces of the two rings. It keeps the plastic ring fixed while a sliding motion occurs with the rotating metal ring connected to the mixer shaft.

Figure 1 shows the seal assembly where the ring made in polyester is represented in green color. The metal ring is produced by turning a mechanical tube made of steel (Fe 510) and it has an external and internal diameter of 170 mm and 123 mm respectively and a slope of the upper face equal to  $25^\circ$ . It is fixed to the shaft of the mixer using a shrink disk, that is inserted into the conical cavity inside the ring. The shrink disc forces the ring to rotate continuously with the shaft. A carbonitriding surface treatment [21] is applied to the tapered face of the ring where sliding occurs to enhance wear and friction resistance. This treatment employs a material thickness that is less than 1 mm, and a subsequent grinding process decreases the surface roughness of the face, reducing friction. The plastic ring is made of polyester, a material suitable for applications requiring mechanical and chemical resistance. It is particularly suitable for parts subjected to wear and abrasion [22]. It has an external diameter of 205 mm, an inner diameter of 131 mm and 10 mm thickness. This ring is fixed to the shaft support through four holes on its surface, through which the anchoring screws of the coupling ring pass.

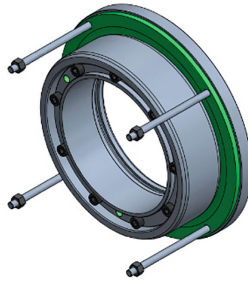


**Fig. 1.** The analyzed mechanical face seals: in green the ring made in polyester.

When the screws are tightened, the plastic ring is forced against the tapered surface of the metal ring and is forced to deform, as represented in Fig. 2.

Two channels are created on the surface of the plastic ring in contact with the metal ring which allow the penetration of the grease throughout the contact area between the two faces. The lubricant is forced by the pump with the necessary overpressure to allow the lubricant penetration at the seal's interface. The pump works in on-off cycles of two minutes. The on-off phases prevent a big amount of grease from the seals from contaminating the processed concrete. By reducing the grease pumping time, the concrete's final quality is preserved, but this causes abrasive wear of the seals during the periods when the pump is turned off due to lack of lubrication and penetration of the mixture into the interface.



**Fig. 2.** Section of the mounted seal: in green the ring made in polyester.

## 2.2 Worn Mechanical Face Seal

Figure 3 shows the worn surfaces of the two rings of the seal at the end of its life: the worn metal ring (on left) and the worn plastic ring (on right). One can observe that wear is predominant on the metal ring and that on the plastic ring contact surface (the inner portion) there is a concave area due to a permanent deformation of the plastic material imprinted by the truncated conical surface of the metal ring. Noticeable marks are present on the ring's central surface, caused by the degradation of the polyester due to contact with contaminants. The contamination is most likely due to concrete deposits in the seal's grooves.





**Fig. 3.** The worn rings of the mechanical face seal.

## 3 Experimental Evaluations

### 3.1 3D Model of the Worn Metal Ring

Digital wear evaluation methods are included in the typical techniques of digital tribology and are performed by 3D digital instruments and software such as 3D optical non-contact scanners or high-precision contact digitizers combined with post-processing and inspection software. Figure 4 shows the 3D scanner used to digitize the entire surface of the component which is a 3D laser scanner mounted on an articulated arm and combined with a CMM (Contact Measuring Machine) probe.

Considering that the wear of the plastic ring is negligible compared to that of the metal ring, the experimental and wear analysis was conducted on the metal ring.

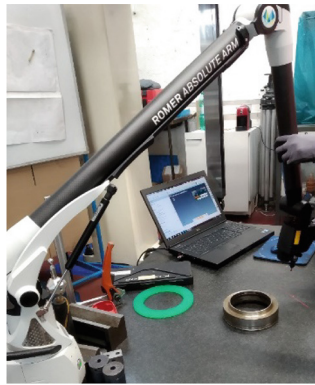


**Fig. 4.** The 3D scanner mounted on arm.

The scanning of the worn metal ring was performed by moving the 3D scanner around the object and obtaining the real time digital model in a workspace with the absolute coordinates provided by the arm. A point cloud was obtained, which was converted into a polygonal surface (mesh) during the post-processing. Therefore, geometries and measures of the features of interest were obtained and the component was digitally reconstructed as shown in Fig. 5.



**Fig. 5.** 3D digital model of the worn metal ring obtained by 3D scanning.

### 3.2 Digital Wear Evaluation Method

Recently, digital wear evaluation methods have received increasing attention, both due to new digital technical knowledge [22–25] and to the ease of application compared to other methods. The digital wear evaluation method used in this paper implied the comparison between the model from the 3D scanning procedure and a reference CAD (Computer Aided Design) model representing the new, unworn component. This comparison was performed by aligning the two models based on the unworn surfaces and evaluating a quantitative 3D wear map displaying the distribution of wear over the entire component's surface. Moreover, with this method to evaluate 3D wear progress, all the wear parameters can be measured obtaining further information about wear depths, volumes of worn material and wear rates.

As a result, cross-sections of the aligned worn and unworn ring were taken at various radial planes on the 3D model to establish the average wear profile and displaying the worn area. Figure 6 shows the final worn profile in green and the unworn profile in black.



**Fig. 6.** Unworn profile (black) and final worn profile (green) of metal ring.

### 3.3 Analysis

From the results analysis, it results that the wear phenomenon arises in three main different phases:

- **Phase I:** Wear occurs by maintaining conformal contact that allows for regular functioning of the seal during the phase in which the lubricant generates the fluid film.

- **Phase II:** Wear is due to the reduction in pressure and the consequent penetration of concrete between the two rings.
- **Phase III:** This is a destructive and final phase that leaves the seal unable to work properly.

**Phase I.** During the first phase, the seal works properly. The removal of material from the metal ring is mainly due to the friction between the two tapered faces of the rings when the grease pump is switched off. Figure 7 shows the section of the wear volume during the first phase. During this phase a certain amount of processed concrete particles starts accumulating inside the seal, as Fig. 8 shows.

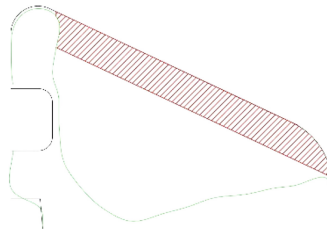


**Fig. 7.** Section of wear volume during the first phase.



**Fig. 8.** Concrete particles accumulation zones inside the seal.

**Phase II.** This is the phase in which most of the material is removed (Fig. 9). It can be observed how the surface contact decreases and at the end of this phase, a “support tooth” is formed in the outermost part. At this stage, the wear is due to the reduction in pressure from the coupling rings and the consequent penetration of concrete material between the two rings. As the plastic ring is not supported by the metal ring (because it is being worn), a rotation occurs and at the end of this phase, the plastic ring is flat. At this point, the third phase begins.

**Phase III.** This is a destructive phase that completes the obtained worn profile (Fig. 10). The seal is completely damaged and is no longer able to avoid the inlet of concrete particles at the rings interface. The high hardness of the concrete conglomerates, together with the high motor torque generate a serious decay. At this stage there is the risk that the concrete impurities could pass through the sealing zone reaching and damaging other organs of the machinery, such as shaft bearings.

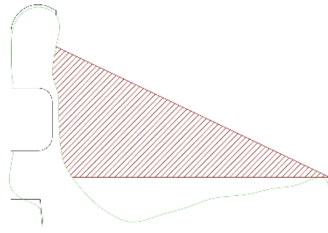


**Fig. 9.** Section of wear volume during the second phase.

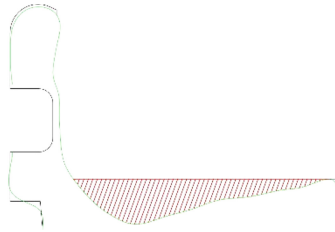


**Fig. 10.** Section of wear volume during the third phase.

For the wear volume calculation corresponding to the three phases the worn profile was simplified generating an approximated regular curve fitting with the real curve.

The aggregates used into the various concrete recipes are classified by the regulation UNI EN 12620:2008 which establishes that the determination of the granulometry must be done by sifting. Aggregates are classified into thin or thick based on the maximum and minimum dimension of the grains, respectively  $D$  and  $d$ . In particular, thin aggregates can have particles with dimensions lesser than 1 mm and can accumulate inside small gaps at the seal's interface scratching the surfaces during the rotation. These particles have a high hardness and contribute to increasing the wear progress. The wear analysis was also completed by gravimetric tests on the new and completely worn metal ring to determine the wear volumes to compare with the results of the 3D wear analysis.

### 3.4 Results

Wear volumes related to the three detected wear phases were determined and compared to the volume of the worn material obtained by the gravimetric test on the metal ring and considering the density of  $7.87 \text{ g/cm}^3$  and the volume of the unworn metal ring equal to  $385616 \text{ mm}^3$ . Table 1 shows the wear results of the three detected phases in terms of loss of material in terms of volume and wear rates. Table 2 reports the comparison of results obtained by 3D scanning and gravimetric methods.

Results of Table 1 corresponding to the three phases agree with the hypotheses that during the first phase, the seal can still work properly and that there is not a catastrophic removal of material. Then the wear rate due to the second phase demonstrates that there is a penetration of the slurry particles inside the mating surfaces which causes a rapid

decay of the surfaces and conducts to phase three, where a lower wear rate corresponds to the catastrophic brake of the metallic ring.

**Table 1.** Wear volumes and rates from the 3D scanning experiments.

Wear Contribution	Wear Volume [mm <sup>3</sup> ]	Wear Rate [%]
Phase I	23860	6.19
Phase II	41774	10.83
Phase III	14614	3.79

**Table 2.** Comparison of gravimetric and digital data.

Wear Contribution	Wear Volume [mm <sup>3</sup> ]	Wear Rate [%]
Gravimetric test	80051	20.76
3D digitization test	80248	20.81

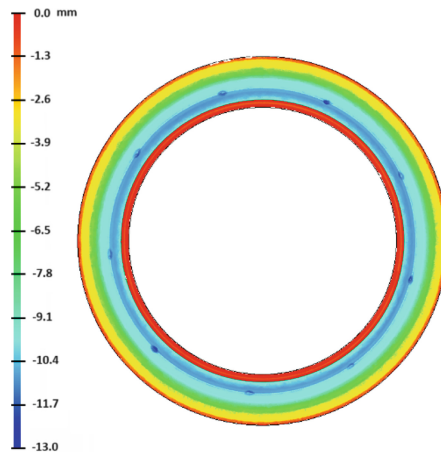


**Fig. 11.** 3D wear map of the metal ring.

The mitigation of wear, especially in the last two phases, can be obtained by limiting the inlet of solid particles into the sealing interface and this can be achieved for instance by controlling the pressure inside the sealing chamber. Furthermore, results reported in Table 2 show that the percentage error between the gravimetric and 3D digitization tests is 0.24% and therefore that the proposed method is suitable for studying wear in these conditions and with respect to the gravimetric method it allows to detect the 3D wear distribution over the metal ring surface as represented in Fig. 11. This wear map shows the wear depth with respect to the base plane of the metal ring. One can observe that the wear distribution is circumferentially quite uniform. Dark blue spots on the wear map correspond to nine screw holes which intersect the final worn surface.

## 4 Conclusions and Future Developments

In this paper, the wear behaviour of a mechanical face seal for twin-shaft concrete mixers was analysed by 3D digitization instruments and methods. Specifically, a metrology-grade 3D laser scanner was employed to reconstruct the 3D digital model of the worn metal ring of the seal which results as the most worn component. In addition, 3D post-processing and aligning methods allowed to display the worn profile and the 3D wear map of the component. Based on the analysis of the wear profiles, three different wear phases were defined resulting in three different wear volumes and behaviour. Resultant wear volumes and rates were also compared with results from gravimetric tests finding an average error of 0.24%. Results of this paper lay the groundwork for a future model of the wear behaviour of mechanical face seals in twin-shaft concrete mixers. Furthermore, the analysis of the wear causes and behaviours will be useful to propose solutions to limit and control the wear phenomena. For instance, a solution based on a pressurized sealing chamber is going to be investigated to allow a continuous operation of the pump avoiding the input of grease into the tank. In addition, the application of a sensor that discriminates the switch between the three detected wear phases is going to be evaluated.

## References

1. Braccesi, C., Valigi, M.C.: Undesired acoustic emissions of mechanical face seals: model and simulations. *Tribol. Int.* **71**, 125–131 (2014)
2. Logozzo, S., Valigi, M.C.: Investigation of instabilities in mechanical face seals: prediction of critical speed values. In: Uhl, T. (eds.) *IFTToMM WC 2019. MMS*, vol. 73, pp. 3865–3872. Springer, Cham (2019). [https://doi.org/10.1007/978-3-030-20131-9\\_383](https://doi.org/10.1007/978-3-030-20131-9_383)
3. Valigi, M.C., Braccesi, C., Cianetti, C., Logozzo, S.: Stick-slip simulation and detection in mechanical face seals. In: *ASME International Mechanical Engineering Congress and Exposition*, vol. 57588, pp. V015T19A033. American Society of Mechanical Engineers (2015)
4. Valigi, M.C., Braccesi, C., Logozzo, S.: A parametric study on friction instabilities in mechanical face seals. *Tribol. Trans.* **59**(5), 911–922 (2016)
5. Valigi, M.C., Braccesi, C., Logozzo, S., Conti, L., Borasso, M.: A new telemetry system for measuring the rotating ring's temperature in a tribological test rig for mechanical face seals. *Tribol. Int.* **106**, 71–77 (2017)
6. Yin, Y., Liu, X., Huang, W., Liu, Y., Hu, S.: Gas face seal status estimation based on acoustic emission monitoring and support vector machine regression. *Adv. Mech. Eng.* **12**(5), 1687814020921323 (2020)
7. Valigi, M.C., Logozzo, S., Braccesi, C.: Contact models and reduction of instabilities in sealing rings for sustainability purposes. In: *Proceedings of I4SDG Workshop 2021: IFTToMM for Sustainable Development Goals*, vol. 1, pp. 412–420 (2022)
8. Maculotti, G., Goti, E., Genta, G., Mazza, L., Galetti, M.: Uncertainty-based comparison of conventional and surface topography-based methods for wear volume evaluation in pin-on-disc tribological test. *Tribol. Int.* **165**, 107260 (2022)
9. Valigi, M.C., Logozzo, S., Landi, L., Braccesi, C., Galletti, L.: Twin-shaft mixers' mechanical behavior numerical simulations of the mix and phases. *Machines* **7**(2), 39 (2019)
10. Valigi, M.C., Logozzo, S., Galletti, L.: Effect of design parameters and operating conditions in concrete twin shaft mixers. In: Carbone, G., Gasparetto, A. (eds.) *IFTToMM ITALY 2018. MMS*, vol. 68, pp. 424–431. Springer, Cham (2019). [https://doi.org/10.1007/978-3-030-03320-0\\_46](https://doi.org/10.1007/978-3-030-03320-0_46)

11. Niță, A., et al.: Research regarding the effect of mineral aggregates on the wear of mixing blades of concrete mixers. *Materials* **16**(14), 5047 (2023)
12. Valigi, M.C., Fabi, L., Gasperini, I.: Wear resistance of planetary concrete mixer blades. In: *World Tribology Congress 2013*, vol. 2, pp. 1208–1211 (2013). E. Ciulli et al
13. Logozzo, S., Valigi, M.C.: Wear assessment and reduction for sustainability: some applications. In: Quaglia, G., Gasparetto, A., Petuya, V., Carbone, G. (eds.) *I4SDG 2021. MMS*, vol. 108, pp. 395–402. Springer, Cham (2022). [https://doi.org/10.1007/978-3-030-87383-7\\_43](https://doi.org/10.1007/978-3-030-87383-7_43)
14. Valigi, M.C., Logozzo, S., Rinchi, M.: Wear resistance of blades in planetary concrete mixers. Part II: 3D validation of a new mixing blade design and efficiency evaluation. *Tribol. Int.* **103**, 37–44 (2016)
15. Valigi, M.C., Logozzo, S., Canella, G.: A robotic 3D vision system for automatic cranial prostheses inspection. In: Ferraresi, C., Quaglia, G. (eds.) *RAAD 2017. MMS*, vol. 49, pp. 328–335. Springer, Cham (2018). [https://doi.org/10.1007/978-3-319-61276-8\\_36](https://doi.org/10.1007/978-3-319-61276-8_36)
16. Valigi, M.C., Logozzo, S., Meli, E., Rindi, A.: New instrumented trolleys and a procedure for automatic 3D optical inspection of railways. *Sensors* **20**(10), 2927 (2020)
17. Logozzo, S., Valigi, M.C., Malvezzi, M.: Modelling the human touch: a basic study for haptic technology. *Tribol. Int.* **166**, 107352 (2022)
18. Affatato, S., Ruggiero, A., Logozzo, S.: Metal transfer evaluation on ceramic biocomponents: a protocol based on 3D scanners. *Measurement* **173**, 108574 (2021)
19. Affatato, S., Valigi, M.C., Logozzo, S.: Knee wear assessment: 3D scanners used as a consolidated procedure. *Materials* **13**(10), 2349 (2020)
20. Pawlus, P., Reizer, R.: Profilometric measurements of wear scars: a review. *Wear* 205150 (2023)
21. <https://www.gruppogaser.com/news/carbonitrurazione-14>
22. Cosenza, C., Malfi, P., Nicoletta, A., Niola, V., Savino, S., Spirito, M.: Experimental approach to study the tribological state of gearwheel through vision devices. *Int. J. Mech. Control* **24**(1), 61–68 (2023)
23. Logozzo, S., Valigi, M.C.: Green tribology: wear evaluation methods for sustainability purposes. *Int. J. Mech. Control* **23**(1), 23–33 (2022)
24. Yang, K., et al.: Design of the fall-block sensing of the railway line pantograph based on 3D machine vision sensors. *Sensors (Switzerland)* **18**(7) (2018). Art. no. 2305
25. Castriota, A., De Giorgi, M., Manco, F., Morabito, A., Nobile, R.: A semi-automatic methodology for tire's wear evaluation. *Meas. Control* **56**(7–8), 1292–1307 (2023)



# Clarification of the Corrosion and Frictional Behavior of Nitrogen-Doped ta-C Coating in Nitride Acid Solution

Ruixi Zhang<sup>(✉)</sup>, Haodong Feng, Noritsugu Umehara, and Takayuki Tokoroyama

Department of Micro-Nano Mechanical Science and Engineering, Graduate School of Engineering, Nagoya University, Nagoya 464-8603, Japan

ruixi.zhang@mae.nagoya-u.ac.jp

**Abstract.** The ta-C coating, characterized by a high fraction of  $sp^3$  hybridized structure, was considered as a potential protective film for preventing bearing steel corrosion in acidic environments due to its chemical inertness. In this study, it was suggested that incorporating nitrogen into the ta-C coating could increase fracture toughness, ultimately enhancing corrosion resistance and frictional performance in nitric acid solutions. As the nitric acid solution's concentration increased to pH1, the surface of the ta-C coating exhibited a significant increase in cracks and pitting. Raman spectroscopy revealed the incorporation of nitrogen resulted in an increased  $sp^2$  structure, enhancing electronic conductivity, and inversely reducing the corrosion resistance of the ta-C coating in the acid solution. SEM observation unveiled the corrosion process, involving small pitting, crack propagation, and delamination. Ultimately, the rough surface corroded by pH1  $HNO_3$  solution resulted in a higher friction coefficient of 0.083 (with  $Si_3N_4$  ball as the counterpart), indicating the compromised efficacy of the ta-C coating under pH1 conditions.

**Keywords:** acid solution · corrosion resistance · friction · nitrogen-dopant · ta-C coating

## 1 Introduction

In the automotive industry, emissions from vehicle exhaust, especially the release of particulate matter, are widely recognized as a significant contributor to air pollution [1–3]. Globally, most countries have enacted emission regulations to reduce vehicle exhaust emissions and address environmental pollution [4, 5]. One effective approach to reducing nitrogen oxides ( $NO_x$ ) emissions from diesel engines is through exhaust gas recirculation (EGR), which involves reducing the oxygen in the cylinder, consequently lowering the combustion temperature [6–8].

Increasing the EGR rate has a positive impact on reducing  $NO_x$  emissions; however, it also has a negative effect by increasing particulate matter and other pollutant components. Diesel combustion generates corrosive gases like sulfur and nitrogen, along with carbonaceous particles that contribute to valve wear [9–12]. During the EGR process,



these corrosive gases enter the engine's intake and exhaust systems, as well as EGR pipelines, where they condense and form highly corrosive media such as sulfuric acid and nitric acid. This significantly weakens the reliability of the EGR system and leads to corrosion damage in internal engine components.

Simultaneously, nitric acid ( $\text{HNO}_3$ ) plays a crucial role as a chemical raw material in the production, storage, and transportation processes of various stainless-steel components, including valves, bearings, and blades [13, 14]. These components frequently encounter challenges from interactions with acidic corrosive media and undergo frictional wear, posing reliability and safety hazards during service. Therefore, the development of surface protection methods for key components exposed to acidic corrosive media is essential. These methods should meet the requirements of acid resistance while also delivering excellent anti-friction and wear-resistant properties.

In practical working conditions, ta-C coatings (tetrahedral amorphous carbon) [15–22] are exposed to various corrosive media, including bodily fluids in the biomedical field, seawater in marine and offshore applications, cutting fluids in the machining field, and more. The presence of corrosive media accelerates the failure of thin films and can lead to severe damage to protective coatings. DLC itself is insulated and exhibits good chemical inertness and stability, making it resistant to corrosion. [23] However, corrosion damage to DLC coating primarily arises from defects, pinholes, significant compositional inhomogeneity, or localized stress concentration [24–27].

Through literature reviews, it is noted that the development and improvement of DLC coating on corrosion resistance can be carried out based on the aspects mentioned beforehand. Consequently, there is rarely research that investigates both the corrosion resistance and the frictional behavior of ta-C in aqueous  $\text{HNO}_3$  solutions. Therefore, this study aims to clarify the corrosion mechanism and its influence on the friction performance in  $\text{HNO}_3$  solutions. Additionally, the doping effect of nitrogen on the corrosion resistance of ta-C coating will be figured out.

## 2 Materials and Methods

### 2.1 Specimen Preparation

The ta-C films investigated in this research were deposited by the ion beam assisted-filtered arc deposition (IBA-FAD) equipment, as illustrated in Fig. 1. The hybrid film deposition system allows the simultaneous deposition of carbon film (employed by T-shaped filtered cathodic vacuum arc deposition, VACS-110H purchased from Onward Giken Co., Ltd.) and other elements (Ti interlayer in the research, employed by unbalanced magnetron sputtering). In addition, the nitrogen element was introduced with the form of ion beam irradiation, using the GG12 ion gun from ADL Co., Ltd. A mirror finished SUJ2 disk (ISO B1 Bearing Steel,  $\Phi 22.5$  mm, thickness 4 mm, surface roughness  $R_a$  below  $0.01 \mu\text{m}$ , HRC60 or higher) was utilized as the substrate. The SUJ2 substrate was ultrasonically cleaned with benzene and acetone for 15 min each, to remove the contaminants on the surface. The chamber was initially vacuumed to  $\sim 0.004$  Pa, and the working pressure fluctuated near 0.02 Pa during the deposition process.

The deposition was conducted in three processes: (1) pre-arc to clean the carbon target and pipe duct. (2) plasma etching performed by ion-gun, (3) Ti interlayer deposited

by magnetron sputtering, and (4) ta-C and ta-CN<sub>x</sub> deposition. In details, Ar plasma was carried out to etch the oxidants and contamination on the surface of SUJ2 disk, introducing the argon gas with the flow rate of 16 sccm and setting the discharge voltage to 1.8 kV. Titanium coating was used as an intermediate layer to prevent delamination because the incompatibility with thermal expansion between DLC coatings and steels can result in inadequate adhesion, as well as increase internal stresses between thin coating and substrate. Argon gas (flow rate of 25 sccm) ionized by glow discharge was forced to collide with the Ti target and Sputtering was carried out for 15 min with a power output of 600 W; and the thickness of Ti-interlayer was 500 nm. The deposition of ta-C coating was carried out with the 80 A of arc discharge current, – 100 V of substrate bias voltage; as well as 4 rpm of the rotation speed of substrate stage. In addition, the nitrogen gas (flow rate of 20 sccm) was introduced using the ion gun with the discharge voltage of 1.0 kV.

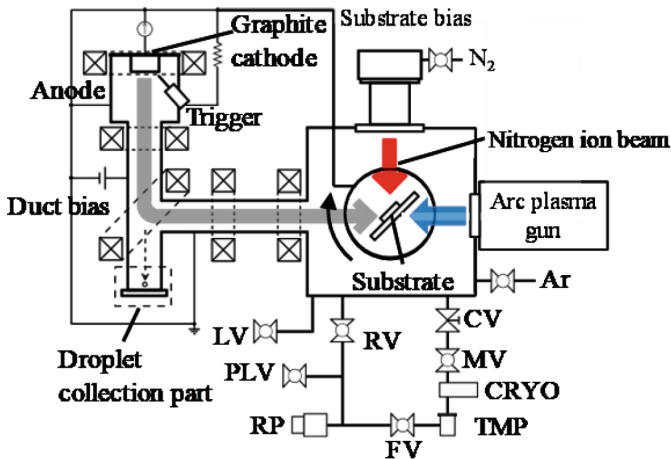
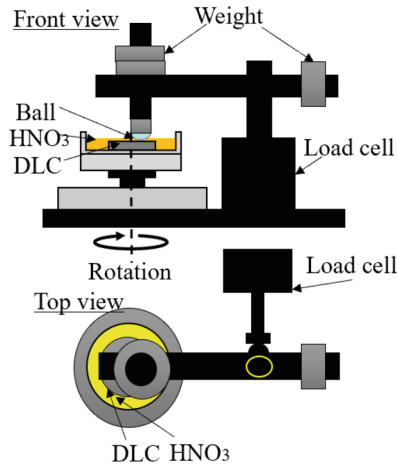


Fig. 1. Schematic diagram of the IBA-FAD hybrid deposition system

## 2.2 Friction Test in the HNO<sub>3</sub> Solution

The tribological properties of ta-C film in HNO<sub>3</sub> solution were investigated using a ball-on-disk friction tester, as shown in Fig. 2. The Si<sub>3</sub>N<sub>4</sub> ball (diameter = 8 mm) was used as the counterpart against ta-C, and the samples were cleaned with acetone in an ultrasonic bath for 15 min. The ta-C disk was rotated with the sliding velocity of 38 mm/s, and the total sliding time lasted for 60 min; the normal load was 4.9 N by vertically applying deadweight to the specimen. The nitric acid solution with various pH value of 1, 2 and 3 was respectively added into the tub prior to the friction test, and the experiment was conducted at a room temperature of 23 °C, with a humidity level of 20%. Each experiment was conducted three times to ensure the credibility.



**Fig. 2.** Schematic diagram of the ball-on-disk friction tester

### 2.3 Electrochemical Test

Electrochemical testing involves measuring the electrochemical reactions occurring at the interface between an electrode and an electrolyte solution, offering valuable insights into corrosion resistance. In this study, the electrochemical corrosion performance of ta-C samples was assessed using the Hokuto Potentiostat electrochemical workstation, which comprises the Potentiostat and a function generator. The Potentiostat was used to control and measure electrochemical reactions, while the function generator generated a linear potential sweep signal for studying oxidation-reduction reactions on the electrodes. In addition, each electrochemical test was conducted three times.

In the Potentiostat's three-electrode system, as shown in Fig. 3, a saturated KCl silver/silver chloride (Ag/AgCl) electrode served as the reference electrode (the standard potential of +0.197 V), providing a known electrochemical potential against which the potential of the working electrode was measured. The counter electrode was a platinum electrode, completing the electrical circuit in the electrochemical cell, with the sample itself serving as the working electrode.

The working electrode, made of PTFE material, had an exposed area of 1.12 cm<sup>2</sup> to the electrolyte, regulated by an O-ring seal, housing the ta-C coating disk. Nitric acid solution was employed as the electrolyte.

### 2.4 Coating Characteristics

The nano-hardness and elastic modulus were evaluated considering the thickness using a Nano-indenter (Elionix ENT-1100a, Japan). The film thickness, surface morphology and wear track of the ta-C disk were observed using a confocal laser scanning microscopy (Olympus OLS5100, Japan) and a Field Emission Scanning Electron Microscopy (FESEM; Hitachi High-Technologies, SU8230, Japan), equipped with an energy-dispersive X-ray spectroscopy (EDS). The SEM observation was carried out at an acceleration voltage of 15 kV with the working distance of 15.0 mm. A laser

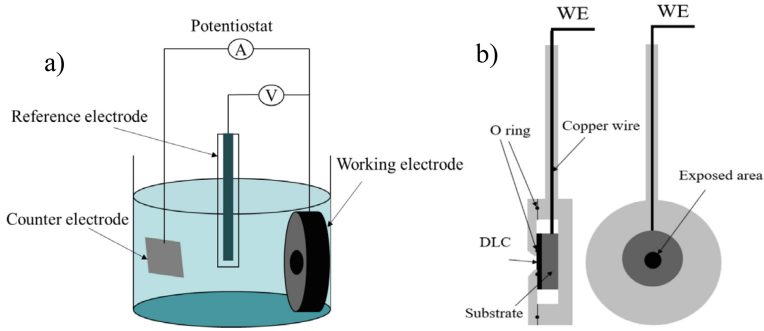


**Fig. 3.** Schematic diagram of a) potentiostat and b) working electrode in the electrochemical workstation, here copper wire was used to connect the disk and potentiostat.

Raman spectroscopy (RENISHAW inVia Reflex, England) was employed to identify the structural transition of ta-C coating with a 532-nm laser and 1800 lines/mm grating.

### 3 Results and Discussions

#### 3.1 Surface Characterization of ta-C Coating

The original surface properties of ta-C and ta-CN<sub>x</sub> coating were shown as listed in Table 1. The ta-C coatings were prepared with thickness of 400 nm, with doping nitrogen element into ta-C coating, the thickness and roughness were hardly changed, whereas, the hardness, as well as Young's modulus were decreased. Immersed in the HNO<sub>3</sub> solution, the surface of ta-C coating was gradually corroded with increasing the concentration, where the poles and defects dramatically increased in the pH1 solution; as demonstrated in Fig. 4. Subsequently, the average roughness was also increased from 0.008 to 1.60 μm when the concentration of HNO<sub>3</sub> solution increased from pH2 to pH1.

**Table 1.** Surface characterization for original ta-C coating

	Thickness, nm	Hardness, GPa	Young's modulus, Gpa	Roughness Ra, μm
ta-C	412	31.3	237.8	0.008
ta-CN <sub>x</sub>	421	12.1	174.3	0.007

#### 3.2 Electrochemical Tests of ta-C Coatings w/o Nitrogen Dopant in HNO<sub>3</sub> Solution

In the immersion test, the challenge of delamination is intricately linked to the fracture toughness of thin films. In this investigation, the incorporation of nitrogen elements

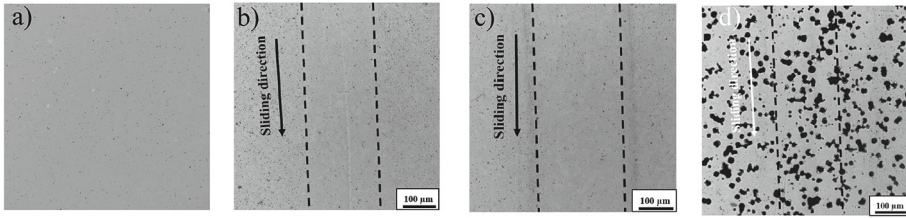


**Fig. 4.** Surface morphology of ta-C coating, immersed in a) no-solution, b) pH3, c) pH2 and d) pH1 of HNO<sub>3</sub> solution, the poles and defects became more while increasing the concentration of HNO<sub>3</sub> solution.

into the ta-C coating was proposed to bolster its fracture toughness, thereby achieving a corrosion-resistant ta-C coating. The extracted values from the examination of polarization curves for ta-C and ta-CN<sub>x</sub>, along with their respective corrosion potential and corrosion current density, are detailed in Table 2. In a pH3 HNO<sub>3</sub> solution, the corrosion current density ( $I_{\text{corr}}$ ) for ta-C and ta-CN<sub>x</sub> was 9.09 and 40.22  $\mu\text{A}/\text{cm}^2$ , respectively. Contrasted with ta-C, ta-CN<sub>x</sub> exhibits a lower corrosion potential, signifying that the corrosion reaction takes place at a lower potential, making it more susceptible to corrosion.

Furthermore, ta-CN<sub>x</sub> displays a higher corrosion current density than ta-C, indicating a greater flow of electric current through the metal surface per unit area. This comparison of both corrosion potential and corrosion current density leads to the conclusion that the corrosion resistance of ta-CN<sub>x</sub> is inferior to that of ta-C.

Raman spectroscopy was employed to determine the carbon structure transition. The  $I_{\text{D}}/I_{\text{G}}$  ratio of ta-C was 0.15, and the  $I_{\text{D}}/I_{\text{G}}$  ratio of ta-CN<sub>x</sub> was 1.06, indicating an increase in sp<sup>2</sup> structure with nitrogen doping. The  $\pi$ -electron cloud in the sp<sup>2</sup> structure enhances electron mobility, making it more conductive, which in turn leads to lower corrosion resistance (Fig. 5).

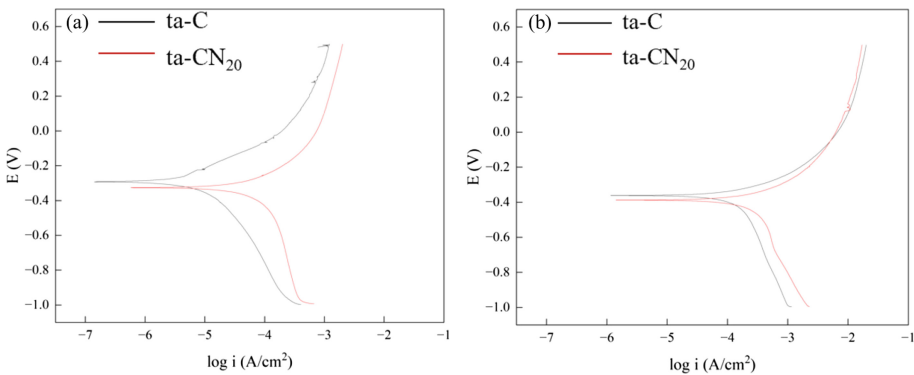


**Fig. 5.** Polarization curves of ta-C & ta-CN<sub>x</sub> coatings in (a) pH3 and (b) pH2 HNO<sub>3</sub> solution

**Table 2.** Corrosion potential and corrosion current density of ta-C and ta-CN<sub>x</sub> coating

	$E_{\text{corr}}$ (V)	$I_{\text{corr}}$ ( $\mu\text{A}/\text{cm}^2$ )
ta-C(pH2)	-0.36	110.41
ta-CN <sub>x</sub> (pH2)	-0.39	195.10
ta-C(pH3)	-0.29	9.09
ta-CN <sub>x</sub> (pH3)	-0.32	40.22

### 3.3 Corrosion Performance and Its Mechanism of ta-C Coating in HNO<sub>3</sub> Solution of pH1

The high concentration of nitric acid solution exacerbated corrosion. Systematic scanning electron microscopy (SEM) observations on the ta-C coating immersed in the pH1 solution enabled us to identify various types of damage morphology, thereby understanding the corrosion performance of the ta-C coating. As shown in Fig. 6, the corrosion process can be speculated to involve the following three steps: (1) crack initiation, (2) crack propagation, and (3) peeling & pitting. Corrosion initiates with the formation of small pitting, allowing aggressive ions to penetrate into the substrate, which can be proved based the corrosion product around the small pitting. At this stage, corrosion gradually expanded to the interlayer and subsequently till the substrate with the form of small pitting, while cracks are simultaneously initiated.

In the second stage, due to the substantial residual internal stress of ta-C coating, cracks propagate, and the pitting area increases as well. During this process, ions became easier to reach the substrate through both pitting and cracks, leading to a significant rise in the corrosion rate. Moreover, residual stress plays a crucial role in ta-C coatings as it significantly affects the stability of these films on substrates.

In the third stage, as the reactive interface layer was gradually dissolved, the advancement of the interface crack front leads to the buckling of the ta-C coating. This buckling phenomenon occurs when the elastic energy stored within the coating surpasses the material's fracture toughness, resulting in the coating's fracture [48]. Simultaneously, due to corrosion, there is no adhesive force between the substrate and ta-C. As a consequence, a crater is formed, leaving behind remnants of the broken coating.

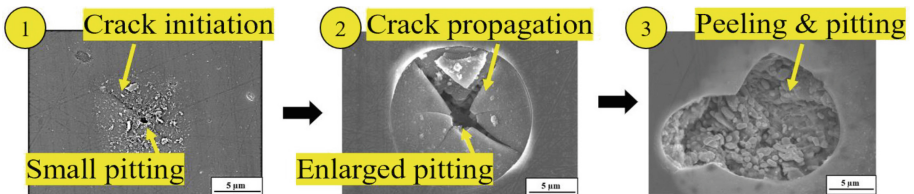


**Fig. 6.** Crack initiation, crack propagation, peeling and pitting behaviors of ta-C coatings in HNO<sub>3</sub> solution of pH1